MIT Open Access Articles

First-principles investigation of organic photovoltaic materials C[subscript 60], C[subscript 70], [C[subscript 60]]PCBM, and bis-[C[subscript 60]]PCBM using a many-body G[subscript 0]W[subscript 0]-Lanczos approach

Massachusetts Institute of Technology

First-principles investigation of organic photovoltaic materials C$_{60}$, C$_{70}$, [C$_{60}$]PCBM, and bis-[C$_{60}$]PCBM using a many-body G_0W_0-Lanczos approach

Xiaofeng Qian,[1,2] Paolo Umari,[3,4] and Nicola Marzari[1,5]

[1]*Department of Materials Science and Engineering, Massachusetts Institute of Technology, Cambridge, Massachusetts 02139, USA*

[2]*Department of Materials Science and Engineering, Texas A&M University, College Station, Texas 77843, USA*

[3]*Dipartimento di Fisica e Astronomia, Universit di Padova, via Marzolo 8, I-35131 Padova, Italy*

[4]*CNR-IOM DEMOCRITOS, Theory@Elettra Group, c/o Sincrotrone Trieste, Area Science Park, Basovizza, I-34012 Trieste, Italy*

[5]*Theory and Simulations of Materials (THEOS), and National Center for Computational Design and Discovery of Novel Materials (MARVEL), École Polytechnique Fédérale de Lausanne, 1015 Lausanne, Switzerland*

We present a first-principles investigation of the excited-state properties of electron acceptors in organic photovoltaics including C$_{60}$, C$_{70}$, [6,6]-phenyl-C$_{61}$-butyric-acid-methyl-ester ([C$_{60}$]PCBM), and bis-[C$_{60}$]PCBM using many-body perturbation theory within the Hedin's G_0W_0 approximation and an efficient Lanczos approach. Calculated vertical ionization potentials (VIP) and vertical electron affinities (VEA) of C$_{60}$ and C$_{70}$ agree very well with experimental values measured in the gas phase. The density of states of all three molecules is also compared to photoemission and inverse photoemission spectra measured on thin films, and they exhibit a close agreement—a rigid energy-gap renormalization owing to intermolecular interactions in the thin films. In addition, it is shown that the low-lying unoccupied states of [C$_{60}$]PCBM are all derived from the highest-occupied molecular orbitals and the lowest-unoccupied molecular orbitals of fullerene C$_{60}$. The functional side group in [C$_{60}$]PCBM introduces a slight electron transfer to the fullerene cage, resulting in small decreases of both VIP and VEA. This small change of VEA provides a solid justification for the increase of open-circuit voltage when replacing fullerene C$_{60}$ with [C$_{60}$]PCBM as the electron acceptor in bulk heterojunction polymer solar cells.

I. INTRODUCTION

Organic photovoltaics (OPV), especially bulk heterojunction (BHJ) type [1,2], are becoming a very promising alternative to the traditional silicon solar cell technology since the former can provide renewable, sustainable, and low-cost clean energy [3–11]. The power conversion efficiency of BHJ-OPV has greatly improved over the last decade from 1% to more than 9% by tuning morphology and blending ratio [12–23], reducing interfacial power losses [24,25], increasing the range of light absorption with tandem cell architecture [26–31], optimizing energy levels, carrier mobility, and optical absorption of low-band-gap polymers [32–48] and fullerenes and their derivatives [43,49–55], and improving device structures [56,57]. In the BHJ type of OPV, low-band-gap polymers not only serve as electron donors but also play several important roles in exciton generation upon light absorption, exciton migration and recombination, and hole transport. Therefore, extensive efforts have been made to enhance sunlight absorption in polymers and increase open-circuit voltage (V$_{oc}$) by lowering the highest-occupied molecular orbital (HOMO) of polymers.

In contrast, fullerenes (C$_{60}$, C$_{70}$) and their derivatives, such as [6,6]-phenyl-C$_{61}$-butyric-acid-methyl-ester ([C$_{60}$]PCBM) and bis-[C$_{60}$]PCBM are often used as electron acceptors in OPV due to their large electron affinities and high electron mobilities. It is known from experimental results that [C$_{60}$]PCBM not only improves the solubility of pure fullerenes but also helps increase the open-circuit voltage [58].

However, the fundamental mechanism of how the functional side group of [C$_{60}$]PCBM affects the V$_{oc}$ is not yet fully understood. In principle, the maximum attainable V$_{oc}$ can be expressed as the energy difference between the lowest-unoccupied molecular orbital (LUMO) level of the electron acceptor and that of the HOMO of the electron donor. It is therefore interesting to see if the theoretically predicted LUMO levels for electron acceptors can account for the difference in V$_{oc}$ reported in experiments.

A few theoretical works, based on density-functional theory (DFT), have been carried out in the past to look into the electronic structure of the above electron acceptors [59–61] leading to a good description of their structural properties. However, the evaluation through DFT of electronic properties such as quasiparticle (QP) energy levels yields results only in qualitative agreement with experiment. High-level quantum chemistry approach and many-body perturbation theory are state-of-the-art methods which can go beyond DFT and provide accurate predictions for excited-state properties. In the case of QP energies in charged excitations upon electron removal/addition, many-body perturbation theory within Hedin's GW approximation [62–65] is computationally less demanding.

The GW method has already been applied to fullerenes in some theoretical works [66–68]. Here, we use the recently developed many-body GW-Lanczos approach which is particularly effective in reaching numerical convergence [69–73] in large atomic structures without suffering from bottlenecks with respect to summing over a large number of empty Kohn-Sham orbitals. This allows us to calculate the electronic structure of the electron acceptors including C$_{60}$, C$_{70}$, [C$_{60}$]PCBM, and bis-[C$_{60}$]PCBM at both the DFT and GW level and compare them with experimental photoemission results. Due to the difficulties in modeling extended and possibly nanostructured materials such as [C$_{60}$]PCBM, we focus here on the isolated molecular limit, therefore addressing changes in the position of LUMO levels rather than their actual

values. Having validated the quality of our QP-energy levels we considered the differences in the maximum attainable V_{oc}, with calculated V_{oc} differences at the *GW* level found to be in reasonable agreement with experiment.

II. METHODS

Ground-state DFT calculations were performed using the *pw.x* code of Quantum-ESPRESSO which is based on the plane-wave pseudopotentials scheme. We used orthorhombic supercells of 31.7^3, 31.7^3, $24 \times 19.2 \times 19.2$, and $47.6 \times 34.3 \times 31.7$ Å^3 for C_{60}, C_{70}, $[C_{60}]$PCBM, and bis-$[C_{60}]$PCBM, respectively, the generalized-gradient approximation (GGA) of exchange-correlation functional in the Perdew-Burke-Ernzerhof (PBE) form [74], Troullier-Martins's norm-conserving pseudopotentials, and a plane-wave basis set with a cutoff of 612.3 eV for C_{60} and C_{70} and 816.3 eV for $[C_{60}]$PCBM, and bis-$[C_{60}]$PCBM. Atomic structures were optimized with a residual force threshold of 0.026 eV/Å, and they are displayed in Fig. 1. We considered not only $[C_{60}]$PCBM in its lowest energy configuration, but also a local-minimum metastable structure with an energy of 0.29 eV higher than that of the ground-state structure.

The *GW* QP-energy level E_i for the ith orbital is obtained in the so-called diagonal G_0W_0 scheme through the solution of the following self-consistent single-variable equation:

$$E_i = \epsilon_i - \langle \psi_i | V_{xc} | \psi_i \rangle + \langle \psi_i | \Sigma(E_i) | \psi_i \rangle, \tag{1}$$

where ψ_i and ϵ_i are the ith Kohn-Sham orbital and its Kohn-Sham energy, V_{xc} is the DFT exchange-correlation potential, and Σ is the self-energy operator in the G_0W_0 approximation. As the calculated G_0W_0 QP energy levels depend upon the choice of the exchange-correlation functional in the starting DFT calculation, we calculated QP energy levels from both GGA-PBE and the local-density approximation (LDA) exchange-correlation functional (LDA) in the Perdew-Zunger form (PZ) [75]. For the two sets of calculations we used the same PBE structural parameters. It is worth noticing that QP energy levels of occupied orbitals correspond to vertical ionization potentials (VIPs), while those of unoccupied ones

correspond to vertical electron affinities (VEAs) which are closely related to the open-circuit voltage discussed later.

In order to remove artificial periodic image interactions, we employed truncated Coulomb potentials with a spherical radius cutoff of 15.9, 15.9, 9.6, and 23.8 Å for C_{60}, C_{70}, $[C_{60}]$PCBM, and bis-$[C_{60}]$PCBM, respectively. For bis-$[C_{60}]$PCBM, we checked the convergence with respect to the radius cutoff by performing *GW* calculations starting from LDA and GGA in a smaller cell of $32.0 \times 19.2 \times 19.2$ Å^3 with a smaller radius cutoff of 9.6 Å. We considered the states close to HOMO and LUMO, and observed only an average increase of VIPs and VEAs of 0.03 (0.03) eV for LDA (GGA). This corroborates the choice of a small (9.6 Å) radius cutoff for $[C_{60}]$PCBM and for addressing the entire electronic DOS of bis-$[C_{60}]$PCBM. The *GW* calculations were performed with the *GWL* code described in Refs. [69,70,72,73]. This approach permits calculations for relatively large atomic structures by expanding the polarizability operators on optimal basis sets.

An optimal basis for representing polarizability operator is given by the most important (i.e., corresponding to the largest eigenvalues) eigenvectors of an easy-to-calculate average polarizability operator. This is defined by the products of occupied orbitals with a set of plane waves which were first projected onto the conduction manifold and then orthonormalized. We indicate with E^* the energy cutoff defining one such plane-waves basis set and with q^* the threshold controlling the final number of elements in our polarizability basis. The accuracy of the final *GW* levels depends on the interplay between E^* and q^*. Larger values for E^* yield more accurate results although requiring smaller q^* and hence larger final basis sets. Smaller values for E^* yield less accurate results but require a smaller number of final basis sets, permitting us to afford larger model structures.

We used a parameter E^* of 68.0 eV and a threshold q^* of 1.0 a.u., resulting in 4381, 5645, and 7005 optimal polarizability basis elements for C_{60}, C_{70}, and PCBM, respectively. The slow convergence of the sum over empty states in conventional *GW* implementations is completely avoided by using a Lanczos chain approach. Here chains of 20 Lanczos steps were applied for the polarizability operators, and chains of 120 Lanczos steps were used for the self-energy expectation values. Those were first evaluated on the imaginary energy axis and then analytically continued onto the real one by fitting with a two-pole expansion. Fitting with a three-pole expansion or changing the energy range in the fitting yielded differences of less than 50 meV for the energy levels of frontier orbitals. We estimate a computational accuracy of 0.1 eV for the calculated QP levels with respect to the vacuum level.

III. GW QUASIPARTICLE ENERGY LEVELS

In Tables I and II we compare the calculated VIPs and VEAs of C_{60} and C_{70} with experimental data. In these two cases, it has been possible to resolve single lines in the experimental photoemission spectra other than the first VEA and VIP. Thanks to the lower symmetry of the molecule, the lines corresponding to all the orbitals have been obtained for C_{70}. For simplicity we indicate G_0W_0@LDA (G_0W_0@GGA), the results for G_0W_0 calculated starting from LDA (GGA). We see that the first VIP calculated by G_0W_0@LDA is larger than that
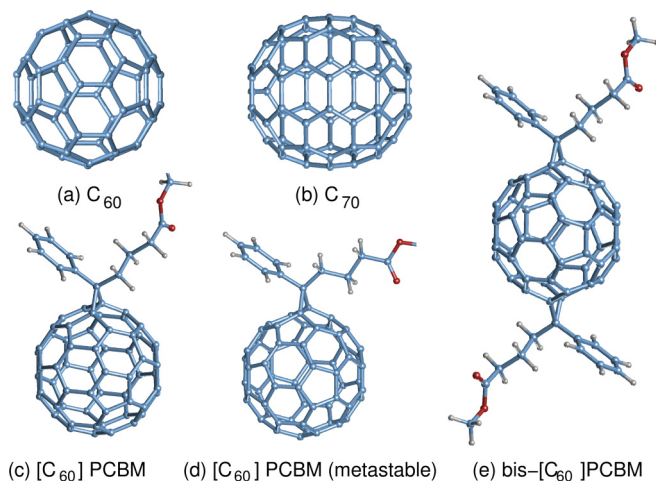

FIG. 1. (Color online) Structure of C_{60}, C_{70}, $[C_{60}]$PCBM, metastable-$[C_{60}]$PCBM, and bis-$[C_{60}]$PCBM.

(a) C_{60} (b) C_{70}

(c) $[C_{60}]$ PCBM   (d) $[C_{60}]$ PCBM (metastable)   (e) bis–$[C_{60}]$PCBM

TABLE I. Low-lying vertical ionization potentials and vertical electron affinities of C_{60} and their corresponding orbitals (units: eV), where we also list the G_0W_0@LDA data of Ref. [68] and G_0W_0@LDA data of Ref. [66].

	Orbital	DFT		G_0W_0				Expt.[76,77]
		LDA	GGA	LDA	LDA [68]	LDA [66]	GGA	
VEA	t_{2u}	2.32	2.17	0.84			0.70	
	t_{1g}	3.21	3.07	1.81			1.65	
	t_{1u}	4.37	4.16	3.04	2.84	3.87	2.82	2.69
	h_u	6.05	5.83	7.68	7.28	8.22	7.37	7.6
	g_g	7.28	6.99	9.01		9.33	8.68	8.95
	h_g	7.40	7.10	9.07		9.42	8.69	
VIP	h_u	8.89	8.63	11.32		11.93	10.94	10.82
	g_u	9.03	8.66	10.65		11.00	10.45	⸮
	t_{2u}	9.60	9.21	11.23		11.46	10.91	11.59
	h_g	9.21	8.93	11.67		12.19	11.25	12.43
	g_u	10.23	9.95	12.76		13.23	12.35	⸮
	t_{1g}	10.75	10.44	13.26		13.60	12.87	
	h_g	10.95	10.50	12.59		12.74	12.33	13.82
E_{gap}		1.68	1.66	4.64	4.44	4.35	4.55	4.91

from G_0W_0@GGA. G_0W_0@LDA overestimates the first VIP up to 0.2 eV for C_{70} while G_0W_0@GGA underestimates it by roughly the same amount. A different trend is found for the first VEAs: Both G_0W_0@LDA and G_0W_0@GGA overestimate the experimental value by about 0.4 eV and 0.2 eV, respectively. This yields similar values in the two approximations for the HOMO-LUMO gaps, which are 0.3 eV lower than experiment. Furthermore, the relative error between higher VIPs and experiment is quite stable and similar to that of the first VIPs, suggesting a good description of the photoemission spectra. Such behavior is not found for DFT calculations, leading to both absolute and relative discrepancies in VIPs and VEAs. In addition, results for ground-state [C_{60}]PCBM, metastable [C_{60}]PCBM, and bis-[C_{60}]PCBM are reported in Tables III, IV, and V. In this case, only the experimental VIP for [C_{60}]PCBM is available, exhibiting the same degree of accuracy as that found for C_{60} and C_{70}.

TABLE II. Low-lying vertical ionization potentials and vertical electron affinities of C_{70} and their corresponding excited states. Units: eV.

	Orbital	DFT		G_0W_0		Expt. [78,79]
		LDA	GGA	LDA	GGA	
VEA	a_1''	4.17	4.00	3.03	2.81	
	e_1''	4.30	4.10	3.13	2.91	2.765
	a_2''	6.14	5.87	7.54	7.21	7.47
	e_1''	6.06	5.82	7.59	7.29	7.47
	a_2'	6.29	6.05	7.88	7.53	7.68
	e_2'	6.42	6.25	8.12	7.79	7.96
	e_2''	6.50	6.16	8.14	7.79	8.12
VIP	e_1'	6.78	6.50	8.44	8.10	8.43
	e_1'	7.53	7.22	9.27	8.87	9.04
	e_2''	7.94	7.61	9.75	9.34	9.28
	e_1''	8.07	7.73	9.93	9.47	9.60
	e_2'	8.15	7.81	9.95	9.54	9.60
	a_1'	8.57	8.21	10.34	9.88	9.84
E_{gap}		1.84	1.77	4.42	4.30	4.71

As listed in Table I for C_{60}, the quantitative description of quasiparticle energies at the G_0W_0 level can be improved by solving the bottleneck of the sum over empty states through the efficient Lanczos approach [69–73]. Indeed, our G_0W_0@LDA results improve upon those of Ref. [66] where a static remainder is used which accounts for infinite sums over empty states [80]. Our G_0W_0@LDA results for VEA and VIP are in a closer agreement with those from Ref. [68] where Gaussian basis sets were used allowing for summing over all the available empty states. Our G_0W_0@LDA VIP and VEA levels are found in the middle between those of Ref. [66] and those of Ref. [68].

The present results are also in good agreement with the predictions from Koopmans' compliant functionals [81,82], where for, e.g., C_{60} using the PBE functional the VIP and VEA are 7.42 eV and 2.82 eV [83], against the present G_0W_0@GGA results of 7.37 eV and 2.82 eV, respectively.

We display in Figs. 2 and 3 the electronic density of states (DOS) of the five electron-acceptor molecules, calculated with

TABLE III. Low-lying vertical ionization potentials and vertical electron affinities of [C_{60}]PCBM and their corresponding excited states. Units: eV.

	Orbital	DFT		G_0W_0		Expt. [60]
		LDA	GGA	LDA	GGA	
VEA		2.61	2.45	1.42	1.18	
	$C_{60}(t_{1g})$	2.84	2.67	1.66	1.44	
		2.87	2.70	1.72	1.49	
		3.77	3.55	2.67	2.40	
	$C_{60}(t_{1u})$	4.00	3.77	2.92	2.64	
		4.03	3.80	2.95	2.69	
		5.53	5.30	7.01	6.72	7.17
		5.67	5.43	7.17	6.88	
VIP	$C_{60}(h_u)$	5.67	5.43	7.14	6.85	
		5.71	5.47	7.21	6.91	
		5.89	5.63	7.38	7.08	
E_{gap}		1.50	1.50	4.06	4.03	

TABLE IV. Low-lying vertical ionization potentials and vertical electron affinities of metastable [C$_{60}$]PCBM and their corresponding excited states. Units: eV.

	Orbital	DFT		G_0W_0		Expt. [60]
		LDA	GGA	LDA	GGA	
VEA	C$_{60}(t_{1g})$	2.85	2.68	1.67	1.41	
		3.08	2.90	1.90	1.67	
		3.11	2.93	1.97	1.73	
	C$_{60}(t_{1u})$	4.00	3.78	2.92	2.63	
		4.24	3.99	3.15	2.85	
		4.27	4.03	3.18	2.94	
VIP	C$_{60}(h_u)$	5.75	5.51	7.24	6.92	7.17
		5.91	5.66	7.41	7.10	
		5.91	5.66	7.36	7.05	
		5.94	5.69	7.44	7.11	
		6.11	5.86	7.61	7.30	
E_{gap}		1.48	1.48	4.06	3.98	

G_0W_0@LDA and G_0W_0@GGA, respectively, and compare them with direct and inverse photoemission data without peak alignment, albeit neglecting any oscillator strength effect in the calculation. We can see that both G_0W_0@LDA and G_0W_0@GGA give a good description of the photoemission spectra. It is worth noting that the lower parts of the conduction DOSs are mainly due to bound orbitals, and they are well described by isolated molecules as can be seen from their excellent agreement with inverse photoemission. In addition, the electronic band gap of thin films is strongly reduced in the bulk with respect to the gas phase, due to the large dielectric screening [84].

It is worth mentioning that [C$_{60}$]PCBM and metastable [C$_{60}$]PCBM exhibit a very similar DOS at both the DFT and the G_0W_0 level with the metastable [C$_{60}$]PCBM shifted by about 0.25 eV towards lower energies. This should be ascribed to the analogous geometry of the two systems accompanied by an increase of the nuclei electrostatic potential for metastable

TABLE V. Low-lying vertical ionization potentials and vertical electron affinities of bis-[C$_{60}$]PCBM and their corresponding excited states. Units: eV.

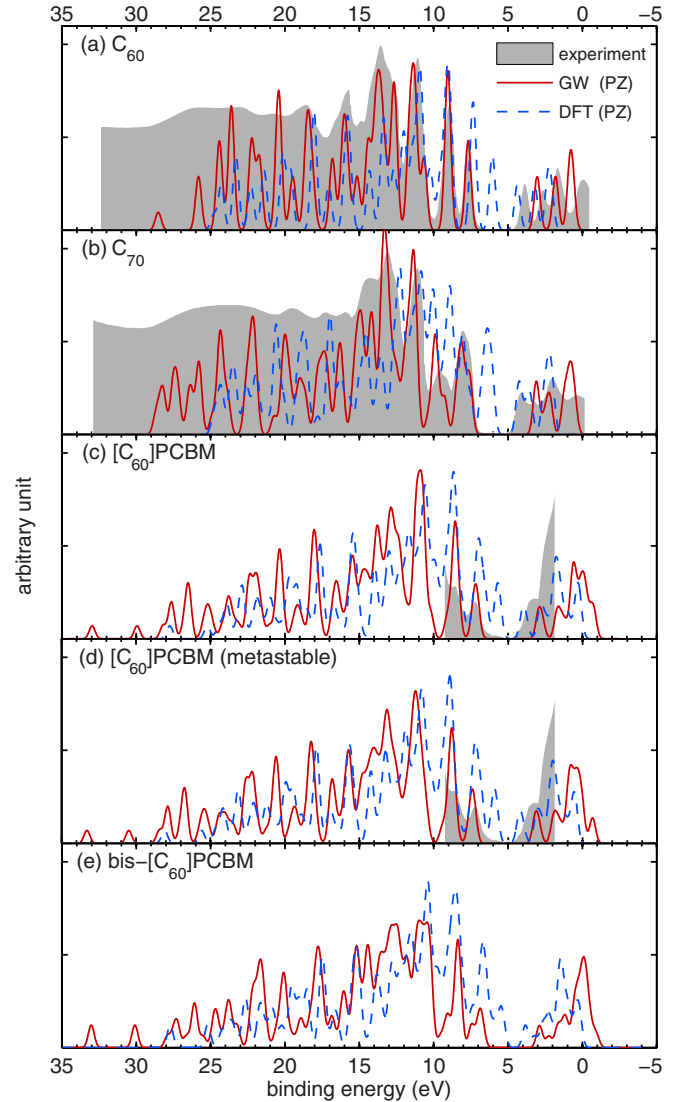|	Orbital	DFT		G_0W_0		Expt. (N.A.)
		LDA	GGA	LDA	GGA	
VEA	C$_{60}(t_{1g})$	2.34	2.19	1.23	1.05	
		2.71	2.53	1.62	1.39	
		2.75	2.58	1.70	1.48	
	C$_{60}(t_{1u})$	3.29	3.08	2.27	2.02	
		3.86	3.62	2.87	2.59	
		3.91	3.68	2.94	2.68	
VIP	C$_{60}(h_u)$	5.35	5.11	6.72	6.42	
		5.52	5.28	6.91	6.59	
		5.53	5.29	6.92	6.60	
		5.61	5.36	7.04	6.72	
		6.00	5.75	7.48	7.16	
E_{gap}		1.44	1.43	3.78	3.74	

FIG. 2. (Color online) Density of states from G_0W_0@LDA and DFT calculations compared with experimental photoemission and inverse photoemission spectra for (a) C$_{60}$, (b) C$_{70}$, (c) [C$_{60}$]PCBM, (d) metastable-[C$_{60}$]PCBM, and (e) bis-[C$_{60}$]PCBM. Experimental data of PES and IPES were adopted from Refs. [85] and [60] for C$_{60}$, C$_{70}$, and [C$_{60}$]PCBM in their thin films, respectively.

[C$_{60}$]PCBM in which the functional group is closer to the C$_{60}$ part than that of ground-state [C$_{60}$]PCBM.

The overall good agreement together with the fact that the main difference with respect to experiments can be described as a rigid shift of the HOMO-LUMO gap by less than about 0.3 eV supports the quality of *GW* results for further investigations of variations in V$_{\mathrm{oc}}$.

IV. ROLE OF SELF-CONSISTENCY AND STARTING DFT FLAVORS

There are two major factors responsible for the difference between G_0W_0 energy levels and experimental values, including the starting DFT flavor and the non-self-consistency of the G_0W_0 scheme. We address these effects by carrying out self-consistent *GW* calculations. In this way, we can single
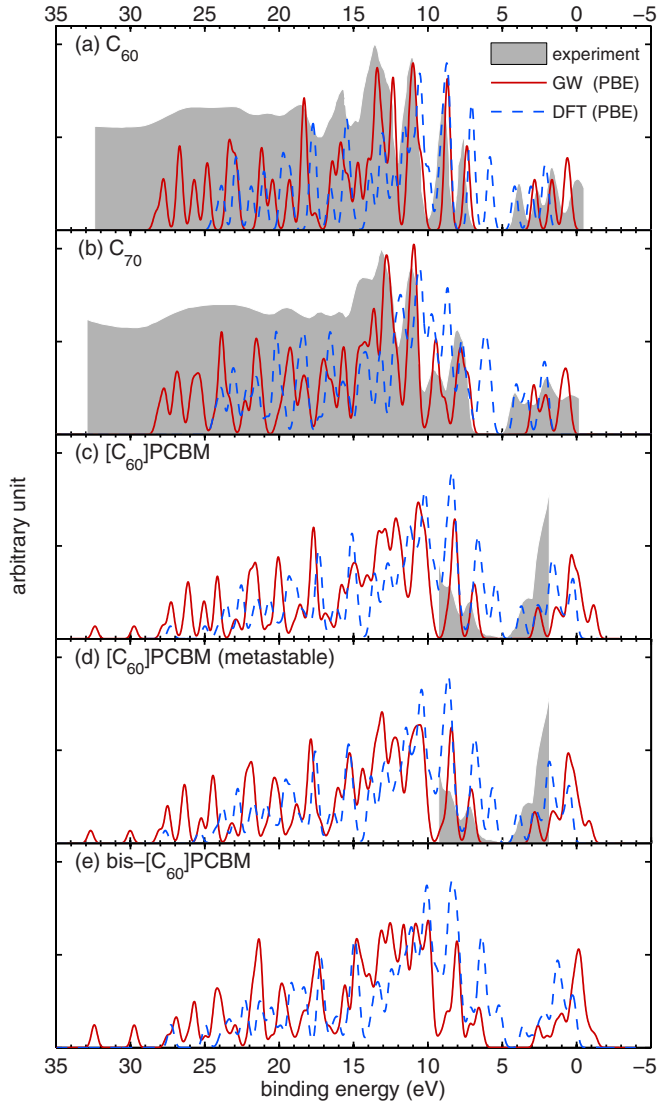
FIG. 3. (Color online) Density of states from G_0W_0@GGA and DFT calculations compared with experimental photoemission and inverse photoemission spectra for (a) C_{60}, (b) C_{70}, (c) [C_{60}]PCBM, (d) metastable-[C_{60}]PCBM, and (e) bis-[C_{60}]PCBM. Experimental data of PES and IPES were adopted from Refs. [85] and [60] for C_{60}, C_{70}, and [C_{60}]PCBM in their thin films, respectively.

out the effects due to different DFT orbitals as we retain the diagonal approximation. We implemented a simplified self-consistent GW scheme. At each iteration, we rigidly displace the energy of the entire valence and the energy of the conduction manifold. In practice, after the first G_0W_0 calculation, we start an iterative series of analogous GW calculations in which all the starting DFT energies of valence states are shifted by s_v and all the starting DFT energies of conduction states are shifted by s_c. This can be achieved by avoiding the sum over empty orbitals through the application of the following operator:

$$\hat{S} = (1 + s_c)\mathbb{I} + (s_v - s_c)\hat{P}_v, \qquad (2)$$

where $\hat{P}_v$ is the projector over the DFT valence manifold and s_v and s_c are chosen in order to align HOMO and LUMO levels with the corresponding GW values of the previous iteration. At

TABLE VI. GW values for VIP and VEA of C_{60} calculated using the self-consistent scheme of Sec. IV. G_nW_n indicates the nth iteration. Units: eV.

		G_0W_0	G_1W_1	G_2W_2	Expt. [76,77]
LDA	VEA	3.04	3.12	3.12	2.69
	VIP	7.69	8.09	8.12	7.6
GGA	VEA	2.82	2.89	2.90	2.69
	VIP	7.37	7.80	7.84	7.6

variance with previous implementations using a rigid scissor [86], it is important not only to update the HOMO-LUMO band gap but also their actual levels as we are interested in the absolute values of the energy levels. For the sake of simplicity, we focus on the VIP and VEA of C_{60} starting from LDA and GGA. The results are reported in Table VI.

We note that VIP and VEA have already converged within a few tens of meV at the second iteration after the first G_0W_0 run. In contrast with G_0W_0, self-consistent GW@GGA gives both VIP and VEA in good agreement (within ∼0.2 eV) with experiment while self-consistent GW@LDA overestimates VIP and VEA by more than 0.4 eV. Moreover, regardless of the LDA or GGA flavor, the GW VEA increases by ∼0.1 eV going from G_0W_0 to self-consistent GW, while VIP increases by ∼0.4 eV. This permits us to ascribe the differences between GW@GGA and GW@LDA to the different quality of the DFT orbitals, i.e., the GGA ones being more accurate.

V. V_{oc} AND THE ROLE OF FUNCTIONAL SIDE GROUP OF PCBM

In actual devices the experimental open-circuit voltage depends not only on the conditions during the measurements (e.g., illumination) but also on the geometry of the cells and the morphology of their constituents. Here, we address only the maximum attainable V_{oc} which, in a single particle picture, is determined by the energy difference between the LUMO level of the electron acceptor and the HOMO level of the electron donor while neglecting structural relaxations accompanying charged excitations. The former corresponds to minus the first-VEA of the acceptor and the latter to minus the first-VIP of the donor. Consequently, V_{oc} = first-VIP (donor) − first-VEA (acceptor). Here, we focus only on the differences in the maximum attainable open-circuit voltage, $\Delta V_{oc}(A|B)$, between electron acceptor A and B. That is, $\Delta V_{oc}(A|B) = V_{oc}(A) - V_{oc}(B)$. Therefore, the comparison with experimental V_{oc}'s would be meaningful only for similar devices.

Quasiparticle energy levels may vary from the limit of an isolated molecule to that of a bulk. In particular, the HOMO-LUMO gap can be significantly reduced [84]. However, in weakly-bonded crystalline or disordered bulks the main effect comes from static dielectric screening. Assuming similar static dielectric properties we can expect similar changes in the LUMO levels. It is also worth noting that the realistic modeling of such electron acceptor layers is quite a demanding task for structural optimization using DFT and electronic structure calculations using the GW approximation. Therefore, it is

TABLE VII. Theoretical and experimental differences in the maximum attainable open-circuit voltage, $\Delta V_{oc}(A|B)$, between electron acceptor A and B (unit: eV). $\Delta V_{oc}(A|B) = V_{oc}(A) - V_{oc}(B)$. We indicate with * the metastable structure of [C_{60}]PCBM.

$\Delta V_{oc}(A\|B)$ (eV)		LDA	GGA	G_0W_0@LDA	G_0W_0@GGA	Expt.
C_{70}	C_{60}	0.08	0.06	-0.09	-0.09	0^a
[C_{60}]PCBM	C_{60}	0.35	0.37	0.09	0.13	0.15^b
[C_{60}]PCBM*	C_{60}	0.11	0.13	-0.15	-0.12	
bis-[C_{60}]PCBM	[C_{60}]PCBM	0.12	0.12	0.01	0.01	0.12^c

[a]Reference [53].
[b]Reference [58].
[c]Averaged value from 0.15 eV of Ref. [51], and 0.23 eV, 0.09 eV, 0.02 eV from Ref. [54].

important to find ways to estimate V_{oc} addressing the limit of isolated systems.

We report in Table VII the differences in the maximum attainable open-circuit voltages, $\Delta V_{oc}(A|B)$. The *GW* calculations can fairly reproduce the experimental ΔV_{oc} for [C_{60}]PCBM taking care of the large range of experimental values. The difference in LUMO energy between C_{60} and [C_{60}]PCBM is small, which can be traced back to the fact that the lowest unoccupied orbitals of [C_{60}]PCBM are derived from the C_{60} three-fold degenerate LUMO. Similarly, the highest occupied orbitals of [C_{60}]PCBM are derived from the C_{60} fivefold degenerate HOMO. These orbitals are displayed in Fig. 4(a) where one can appreciate their localization on the C_{60} group. As highlighted from the Löwdin charge analysis [87] displayed

in Fig. 4(b), a moderate charge transfer of 0.12 *e* occurs towards the fullerene cage. Going from C_{60} to [C_{60}]PCBM, we observe an upshift of the HOMO level and a relatively smaller upshift of the LUMO level, leading to a smaller HOMO-LUMO gap. An analogous behavior is registered from [C_{60}]PCBM to bis-[C_{60}]PCBM where a larger charge transfer is expected.

In contrast, for the metastable [C_{60}]PCBM configuration we predict a lower V_{oc} than for C_{60}. The fair agreement between *GW* and experiment for [C_{60}]PCBM and bis-[C_{60}]PCBM is not observed for C_{70}. In this case, both DFT and *GW* indicate a smaller V_{oc} while experimental V_{oc} shows almost no variation. This must be ascribed to using an isolated molecule approximation, since DFT and *GW* reproduce well the VEA of C_{60} and C_{70} molecules and their order. More accurate results would require the modeling of bulk materials and interfaces.

VI. CONCLUSIONS

GW approaches are very promising for determining the main physical characteristics of polymer solar cells. The isolated molecular limit adopted in this paper gives overall good results, in particular for the [C_{60}]PCBM and bis-[C_{60}]PCBM. These results lead us to expect that more accurate agreement may be obtained by direct modeling of bulk photovoltaic materials and interfaces using the *GW*-Lanczos approach, which is particularly suitable for large systems. Finally, the comparison between ground-state [C_{60}]PCBM and metastable [C_{60}]PCBM demonstrates that the intrinsic morphological difference can have significant effects on the open-circuit voltage, providing a theoretical confirmation of morphology as an important factor in organic photovoltaics.
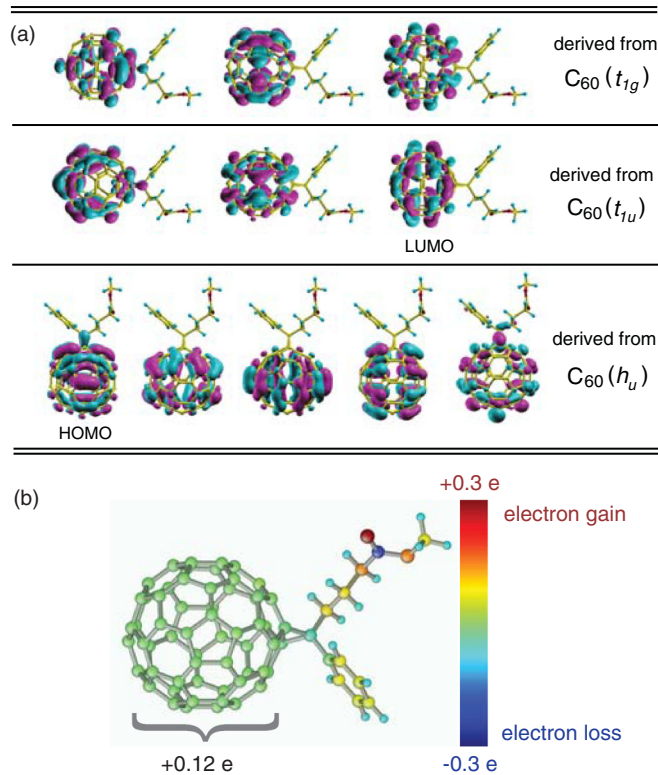
FIG. 4. (Color online) (a) Quasiparticle states close to HOMO and LUMO in the ground-state [C_{60}]PCBM. States shown in the first, second, and third rows are derived from fullerene C_{60}'s t_{1g}, t_{1u}, and h_u, respectively. Purple (cyan) indicates positive (negative) value of wave functions. (b) Löwdin atomic charge analysis of [C_{60}]PCBM. Red (blue) indicates electron gain (loss). About 0.12 electron was transferred from the side group to the fullerene cage.

[1] C. W. Tang, Appl. Phys. Lett. **48**, 183 (1986).

[2] G. Yu, J. Gao, J. C. Hummelen, F. Wudl, and A. J. Heeger, Science **270**, 1789 (1995).

[3] C. J. Brabec, N. S. Sariciftci, and J. C. Hummelen, Adv. Funct. Mater. **11**, 15 (2001).

[4] C. J. Brabec, Sol. Energy Mater. Sol. Cells **83**, 273 (2004).

[5] H. Hoppe and N. S. Sariciftci, J. Mater. Res. **19**, 1924 (2004).

[6] S. Gunes, H. Neugebauer, and N. S. Sariciftci, Chem. Rev. **107**, 1324 (2007).

[7] A. C. Mayer, S. R. Scully, B. E. Hardin, M. W. Rowell, and M. D. McGehee, Mater. Today **10**, 28 (2007).

[8] B. C. Thompson and J. M. J. Frechet, Angew. Chem.-Int. Edit. **47**, 58 (2008).

[9] R. Kroon, M. Lenes, J. C. Hummelen, P. W. M. Blom, and B. De Boer, Polym. Rev. **48**, 531 (2008).

[10] G. Dennler, M. C. Scharber, and C. J. Brabec, Adv. Mater. **21**, 1323 (2009).

[11] C. Deibel and V. Dyakonov, Rep. Prog. Phys. **73**, 096401 (2010).

[12] S. E. Shaheen, C. J. Brabec, N. S. Sariciftci, F. Padinger, T. Fromherz, and J. C. Hummelen, Appl. Phys. Lett. **78**, 841 (2001).

[13] D. Chirvase, J. Parisi, J. C. Hummelen, and V. Dyakonov, Nanotechnology **15**, 1317 (2004).

[14] H. Hoppe, M. Niggemann, C. Winder, J. Kraut, R. Hiesgen, A. Hinsch, D. Meissner, and N. S. Sariciftci, Adv. Funct. Mater. **14**, 1005 (2004).

[15] J. K. J. van Duren, X. N. Yang, J. Loos, C. W. T. Bulle-Lieuwma, A. B. Sieval, J. C. Hummelen, and R. A. J. Janssen, Adv. Funct. Mater. **14**, 425 (2004).

[16] W. L. Ma, C. Y. Yang, X. Gong, K. Lee, and A. J. Heeger, Adv. Funct. Mater. **15**, 1617 (2005).

[17] G. Li, V. Shrotriya, J. S. Huang, Y. Yao, T. Moriarty, K. Emery, and Y. Yang, Nat. Mater. **4**, 864 (2005).

[18] H. Hoppe and N. S. Sariciftci, J. Mater. Chem. **16**, 45 (2006).

[19] Y. Kim, S. Cook, S. M. Tuladhar, S. A. Choulis, J. Nelson, J. R. Durrant, D. D. C. Bradley, M. Giles, I. Mcculloch, C. S. Ha, and M. Ree, Nat. Mater. **5**, 197 (2006).

[20] J. Peet, J. Y. Kim, N. E. Coates, W. L. Ma, D. Moses, A. J. Heeger, and G. C. Bazan, Nat. Mater. **6**, 497 (2007).

[21] A. L. Ayzner, D. D. Wanger, C. J. Tassone, S. H. Tolbert, and B. J. Schwartz, J. Phys. Chem. C **112**, 18711 (2008).

[22] K. Vandewal, A. Gadisa, W. D. Oosterbaan, S. Bertho, F. Banishoeib, I. Van Severen, L. Lutsen, T. J. Cleij, D. Vanderzande, and J. V. Manca, Adv. Funct. Mater. **18**, 2064 (2008).

[23] L. M. Chen, Z. R. Hong, G. Li, and Y. Yang, Adv. Mater. **21**, 1434 (2009).

[24] J. Y. Kim, S. H. Kim, H. H. Lee, K. Lee, W. L. Ma, X. Gong, and A. J. Heeger, Adv. Mater. **18**, 572 (2006).

[25] M. D. Irwin, B. Buchholz, A. W. Hains, R. P. H. Chang, and T. J. Marks, Proc. Natl. Acad. Sci. USA **105**, 2783 (2008).

[26] V. Shrotriya, E. H. E. Wu, G. Li, Y. Yao, and Y. Yang, Appl. Phys. Lett. **88**, 064104 (2006).

[27] K. Kawano, N. Ito, T. Nishimori, and J. Sakai, Appl. Phys. Lett. **88**, 073514 (2006).

[28] A. Hadipour, B. de Boer, J. Wildeman, F. B. Kooistra, J. C. Hummelen, M. G. R. Turbiez, M. M. Wienk, R. A. J. Janssen, and P. W. M. Blom, Adv. Funct. Mater. **16**, 1897 (2006).

[29] J. Gilot, M. M. Wienk, and R. A. J. Janssen, Appl. Phys. Lett. **90**, 143512 (2007).

[30] J. Y. Kim, K. Lee, N. E. Coates, D. Moses, T. Q. Nguyen, M. Dante, and A. J. Heeger, Science **317**, 222 (2007).

[31] T. Ameri, G. Dennler, C. Lungenschmied, and C. J. Brabec, Energy Environ. Sci. **2**, 347 (2009).

[32] K. M. Coakley and M. D. McGehee, Chem. Mat. **16**, 4533 (2004).

[33] D. Muhlbacher, M. Scharber, M. Morana, Z. G. Zhu, D. Waller, R. Gaudiana, and C. Brabec, Adv. Mater. **18**, 2884 (2006).

[34] N. Blouin, A. Michaud, and M. Leclerc, Adv. Mater. **19**, 2295 (2007).

[35] N. Blouin and M. Leclerc, Accounts Chem. Res. **41**, 1110 (2008).

[36] N. Blouin, A. Michaud, D. Gendron, S. Wakim, E. Blair, R. Neagu-Plesu, M. Belletete, G. Durocher, Y. Tao, and M. Leclerc, J. Am. Chem. Soc. **130**, 732 (2008).

[37] J. H. Hou, H. Y. Chen, S. Q. Zhang, G. Li, and Y. Yang, J. Am. Chem. Soc. **130**, 16144 (2008).

[38] Y. F. Li and Y. P. Zou, Adv. Mater. **20**, 2952 (2008).

[39] Y. J. Cheng, S. H. Yang, and C. S. Hsu, Chem. Rev. **109**, 5868 (2009).

[40] J. W. Chen and Y. Cao, Accounts Chem. Res. **42**, 1709 (2009).

[41] F. Flores, J. Ortega, and H. Vazquez, Phys. Chem. Chem. Phys. **11**, 8658 (2009).

[42] Y. J. He and Y. F. Li, Prog. Chem. **21**, 2303 (2009).

[43] S. H. Park, A. Roy, S. Beaupre, S. Cho, N. Coates, J. S. Moon, D. Moses, M. Leclerc, K. Lee, and A. J. Heeger, Nat. Photonics **3**, 297 (2009).

[44] Y. W. Li, L. L. Xue, H. Li, Z. F. Li, B. Xu, S. P. Wen, and W. J. Tian, Macromolecules **42**, 4491 (2009).

[45] Y. Y. Liang, Y. Wu, D. Q. Feng, S. T. Tsai, H. J. Son, G. Li, and L. P. Yu, J. Am. Chem. Soc. **131**, 56 (2009).

[46] Y. P. Zou, D. Gendron, R. Badrou-Aich, A. Najari, Y. Tao, and M. Leclerc, Macromolecules **42**, 2891 (2009).

[47] H. Y. Chen, J. H. Hou, S. Q. Zhang, Y. Y. Liang, G. W. Yang, Y. Yang, L. P. Yu, Y. Wu, and G. Li, Nat. Photonics **3**, 649 (2009).

[48] Y. Liang, Z. Xu, J. Xia, S.-T. Tsai, Y. Wu, G. Li, C. Ray, and L. Yu, Adv. Mater. **22**, E135 (2010).

[49] M. M. Wienk, J. M. Kroon, W. J. H. Verhees, J. Knol, J. C. Hummelen, P. A. van Hal, and R. A. J. Janssen, Angew. Chem.-Int. Edit. **42**, 3371 (2003).

[50] F. B. Kooistra, J. Knol, F. Kastenberg, L. M. Popescu, W. J. H. Verhees, J. M. Kroon, and J. C. Hummelen, Org. Lett. **9**, 551 (2007).

[51] M. Lenes, G. J. A. H. Wetzelaer, F. B. Kooistra, S. C. Veenstra, J. C. Hummelen, and P. W. M. Blom, Adv. Mater. **20**, 2116 (2008).

[52] R. B. Ross, C. M. Cardona, D. M. Guldi, S. G. Sankaranarayanan, M. O. Reese, N. Kopidakis, J. Peet, B. Walker, G. C. Bazan, E. Van Keuren, B. C. Holloway, and M. Drees, Nat. Mater. **8**, 208 (2009).

[53] S. Pfuetzner, J. Meiss, A. Petrich, M. Riede, and K. Leo, App. Phys. Lett. **94**, 223307 (2009).

[54] T. Tromholt, S. A. Gevorgyan, M. Jørgensen, F. C. Krebs, and K. O. Sylvester-Hvid, ACS Appl. Mater. Interfaces **1**, 2768 (2009).

[55] A. A. Y. Guilbert, L. X. Reynolds, A. Bruno, A. MacLachlan, S. P. King, M. A. Faist, E. Pires, J. E. Macdonald, N. Stingelin, S. A. Hague, and J. Nelson, ACS Nano **6**, 3868 (2012).

[56] L. Dou, J. You, J. Yang, C.-C. Chen, Y. He, S. Murase, T. Moriarty, K. Emery, G. Li, and Y. Yang, Nat. Photonics **6**, 180 (2012).

[57] Z. He, C. Zhong, S. Su, M. Xu, H. Wu, and Y. Cao, Nat. Photonics **6**, 591 (2012).

[58] C. J. Brabec, A. Cravino, D. Meissner, N. S. Sariciftci, T. Fromherz, M. T. Rispens, L. Sanchez, and J. C. Hummelen, Adv. Funct. Mater. **11**, 374 (2001).

[59] Z. X. Zhang, P. D. Han, X. G. Liu, J. F. Zhao, H. S. Jia, F. G. Zeng, and B. S. Xu, J. Phys. Chem. C **112**, 19158 (2008).

[60] K. Akaike, K. Kanai, H. Yoshida, J. Tsutsumi, T. Nishi, N. Sato, Y. Ouchi, and K. Seki, J. Appl. Phys. **104**, 023710 (2008).

[61] K. Kanai, K. Akaike, K. Koyasu, K. Sakai, T. Nishi, Y. Kamizuru, T. Nishi, Y. Ouchi, and K. Seki, Appl. Phys. A-Mater. Sci. Process. **95**, 309 (2009).

[62] L. Hedin, Phys. Rev. **139**, A796 (1965).

[63] L. Hedin and S. Lundqvist, in *Solid State Physics*, Vol. 23, edited by F. Seitz and D. Turnbull (Academic, New York, 1969).

[64] G. Strinati, H. J. Mattausch, and W. Hanke, Phys. Rev. Lett. **45**, 290 (1980).

[65] G. Strinati, H. J. Mattausch, and W. Hanke, Phys. Rev. B **25**, 2867 (1982).

[66] M. L. Tiago, P. R. C. Kent, R. Q. Hood, and F. A. Reboredo, J. Chem. Phys. **129**, 084311 (2008).

[67] M. L. Tiago and F. A. Reboredo, Phys. Rev. B **79**, 195410 (2009).

[68] X. Blase, C. Attaccalite, and V. Olevano, Phys. Rev. B **83**, 115103 (2011).

[69] P. Umari, G. Stenuit, and S. Baroni, Phys. Rev. B **79**, 201104 (2009).

[70] P. Umari, G. Stenuit, and S. Baroni, Phys. Rev. B **81**, 115104 (2010).

[71] G. Stenuit, C. Castellarin-Cudia, O. Plekan, V. Feyer, K. C. Prince, A. Goldoni, and P. Umari, Phys. Chem. Chem. Phys. **12**, 10812 (2010).

[72] P. Umari, X. Qian, N. Marzari, G. Stenuit, L. Giacomazzi, and S. Baroni, Phys. Status Solidi B **248**, 527 (2011).

[73] X. Qian, P. Umari, and N. Marzari, Phys. Rev. B **84**, 075103 (2011).

[74] J. P. Perdew, K. Burke, and M. Ernzerhof, Phys. Rev. Lett. **77**, 3865 (1996).

[75] J. P. Perdew and A. Zunger, Phys. Rev. B **23**, 5048 (1981).

[76] X. B. Wang, C. F. Ding, and L. S. Wang, J. Chem. Phys. **110**, 8217 (1999).

[77] D. L. Lichtenberger, K. W. Nebesny, C. D. Ray, D. R. Huffman, and L. D. Lamb, Chem. Phys. Lett. **176**, 203 (1991).

[78] X. B. Wang, H. K. Woo, X. Huang, M. M. Kappes, and L. S. Wang, Phys. Rev. Lett. **96**, 143002 (2006).

[79] D. L. Lichtenberger, M. E. Rempe, and S. B. Gogosha, Chem. Phys. Lett. **198**, 454 (1992).

[80] M. L. Tiago and J. R. Chelikowsky, Phys. Rev. B **73**, 205334 (2006).

[81] I. Dabo, A. Ferretti, N. Poilvert, Y. Li, N. Marzari, and M. Cococcioni, Phys. Rev. B **82**, 115121 (2010).

[82] G. Borghi, A. Ferretti, N. L. Nguyen, I. Dabo, and N. Marzari, Phys. Rev. B **90**, 075135 (2014).

[83] N. L. Nguyen, G. Borghi, A. Ferretti, I. Dabo, and N. Marzari, arXiv:1409.4210.

[84] M. Marsili, P. Umari, G. Di Santo, M. Caputo, M. Panighel, A. Goldoni, M. Kumar, and M. Pedio, Phys. Chem. Chem. Phys. **16**, 27104 (2014).

[85] P. J. Benning, D. M. Poirier, T. R. Ohno, Y. Chen, M. B. Jost, F. Stepniak, G. H. Kroll, J. H. Weaver, J. Fure, and R. E. Smalley, Phys. Rev. B **45**, 6899 (1992).

[86] M. R. Filip and F. Giustino, Phys. Rev. B **90**, 245145 (2014).

[87] X. Qian, J. Li, L. Qi, C.-Z. Wang, T.-L. Chan, Y.-X. Yao, K.-M. Ho, and S. Yip, Phys. Rev. B **78**, 245112 (2008).